Supplementary information for: Sequential changes in ocean circulation and biological export productivity during the last glacial cycle: a model-data study

Cameron M. O'Neill[1], Andrew McC. Hogg[1,2], Michael J. Ellwood[1], Bradley N. Opdyke[1], and Stephen M. Eggins[1]

[1]Research School of Earth Sciences, Australian National University, Canberra, Australia
[2]ARC Centre of Excellence for Climate Extremes, Australian National University, Canberra, Australia

Correspondence to: Cameron O'Neill (cameron.oneill@anu.edu.au)

1 Model forcings

Table S1 shows the sea surface temperature (SST) forcings applied to the SCP-M surface boxes in each MIS, for the purposes of undertaking the model-data experiments as decribed in the main text.

Table S1. Sea surface temperature (SST) forcings in each MIS and model box, averaged from values presented in Kohfeld and Chase (2017). All values are degrees Celsius relative to modern day GLODAP data. Key to boxes: Atlantic (box 1: low latitude/tropical surface ocean; box 2: northern surface ocean; box 7: subpolar southern surface ocean). Pacific-Indian (box 8: low latitude/tropical surface ocean; box 11: subpolar southern surface ocean). Southern Ocean (box 12: surface ocean).

MIS	**Time (ka)**	**Box 1 (±°C)**	**Box 2 (±°C)**	**Box 7 (±°C)**	**Box 8 (±°C)**	**Box 11 (±°C)**	**Box 12 (±°C)**
∼1	0-11.7	-0.08	-0.51	0.44	-0.17	0.44	0.54
∼2	18-29	-1.94	-6.94	-1.91	-2.98	-1.91	-1.23
3	29-57	-2.12	-5.33	-1.99	-2.8	-1.99	-1.44
4	57-71	-2.02	-6.09	-1.93	-2.86	-1.93	-1.12
5a	79.5-84.5	-0.54	-2.52	-0.49	-0.9	-0.49	0.26
5b	84.5-89.5	-0.86	-3.19	-0.86	-1.32	-0.86	-0.44
5c	91-101	-0.38	-2.6	-0.83	-0.81	-0.83	-0.6
5d	104-114	-0.87	-2.42	-1.29	-1.2	-1.29	-0.9
5e	118-128	0.2	0.5	0.19	0.3	0.19	0.12

Table S2 shows forcings for other environmental parameters applied in the model-data experiments described in the main text.

Table S2. Model forcings for MIS across the last glacial cycle. Proxy for Antarctic sea ice extent using ssNa fluxes from the EPICA Dome C ice core (Wolff et al., 2010), used to temporally contour MIS model forcings for salinity (Adkins et al., 2002) and polar Southern Ocean piston velocity. Global ocean salinity is forced to a glacial maximum of +1 psu and the polar Southern Ocean is forced to +2 psu, as modified from Adkins et al. (2002). Ocean volume forced using global relative sea level reconstruction of Rohling et al. (2009). Atmospheric ^{14}C production rate time series for 0-50 ka of Muscheler et al. (2014) . Long-term values assumed for >50 ka (Key, 2001). Reef carbonate flux of carbon from Ridgewell et al. (2003) profiled across the glacial cycle using a curve from Opdyke and Walker (1992).

MIS	Southern Ocean (box 12) piston velocity (m day^{-1})	Ocean volume (% of modern)	Coral reef C flux (x 10^{12} mol C $annum^{-1}$)	^{14}C production (atoms s^{-1})	Salinity ($\pm$ psu)	
					Southern Ocean (box 12)	**Rest of ocean**
$\sim$1	3.92	99.9%	4.3	1.62	0.59	0.3
$\sim$2	2.78	97.5%	-1.6	2.36	1.94	0.97
3	2.75	98%	-0.5	2.25	1.99	0.99
4	2.84	97.9%	0.9	1.82	1.85	0.93
5a	3.35	99.1%	2.1	1.73	1.47	0.73
5b	2.97	98.4%	2.4	1.73	1.71	0.86
5c	3.39	98.9%	3	1.73	0.98	0.49
5d	3.18	99.1%	3.8	1.73	1.32	0.66
5e	4.17	99.8%	4.8	1.73	-0.03	-0.01

2 Data compilation

Table S3 shows atmospheric proxy data averaged into MIS slices.

Table S3. Data for atmospheric CO_2 (Bereiter et al., 2015), atmospheric $\delta^{13}C$ (Eggleston et al., 2016) and atmospheric $\Delta^{14}C$ (Reimer et al., 2009), averaged into MIS time slices.

MIS	**CO_2 (ppm)**	**$\delta^{13}C$ (‰)**	**$\Delta^{14}C$ (‰)**
∼1	272.2±7.8	-6.41±0.09	57.1±47.9
∼2	189.1±3.1	-6.42±0.03	466±80
3	202.6±8.6	-6.55±0.14	517.8±131.5
4	210±9.6	-6.63±0.2	nan
5a	239.2±7	-6.47±0.01	nan
5b	226.6±6.6	-6.47±0.01	nan
5c	240.7±5.3	-6.6±0.08	nan
5d	249.2±9	-6.68±0.03	nan
5e	275.9±3.3	-6.66±0.08	nan

Tables S4-S6 shows ocean $\delta^{13}C$, CO_3^{2-} and $\Delta^{14}C$ proxy data mapped and averaged into SCP-M boxes, and averaged in MIS slices.

Table S4. Ocean $\delta^{13}C$ data (‰) sourced from Oliver et al. (2010), mapped into SCP-M boxes and average for each MIS. Key to boxes: Atlantic (box 1: low latitude/tropical surface ocean; box 2: northern surface ocean; box 3: intermediate ocean; box 4: deep ocean; box 6: abyssal ocean; box 7: subpolar southern surface ocean). Pacific-Indian (box 8: low latitude/tropical surface ocean; box 9: deep ocean; box 10: abyssal ocean; box 11: subpolar southern surface ocean). Southern Ocean (box 5: intermediate-deep; box 12: surface ocean).

MIS	**Box 1**	**Box 2**	**Box 3**	**Box 4**	**Box 5**	**Box 6**	**Box 7**	**Box 8**	**Box 9**	**Box 10**	**Box 11**	**Box 12**
∼1	0.52±1	-0.09±0.6	1±0.6	0.88±0.7	-0.33±0	0.66±0.5	0.61±0.5	1.16±0.8	0.39±0.5	-0.2±0.8	0.34±0.6	0.77±0.2
∼2	0.57±0.9	-0.19±0.5	1.46±0.6	0.86±0.7	-0.91±0	-0.05±0.6	0.08±0.6	0.89±1	-0.03±0.6	-0.54±0.5	0.53±0.5	0.16±0.1
3	0.75±0.8	-0.1±0.5	1.09±0.6	0.75±0.7	-0.82±0.1	0.08±0.9	0.03±0.5	1.22±0.6	0.31±0.4	-0.34±0.8	0.38±0.4	0.1±0.1
4	0.51±1	-0.21±0.6	0.72±0.6	0.87±0.8	-0.73±0.1	0.05±0.6	0.08±0.4	1.03±0.7	0.15±0.4	-0.46±0.6	0.33±0.5	0.34±0
5a	0.66±1.2	-0.28±0.3	0.41±0.5	0.99±0.7	-0.7±0	0.46±0.8	0.28±0.3	1.04±1.2	0.5±0.5	-0.29±0.4	0.41±0.4	0.34±0.1
5b	0.48±1.1	-0.24±0.4	0.24±0.2	0.95±0.7	nan	0.38±0.6	0.35±0.4	1.54±0.4	0.43±0.4	-0.12±0.6	0.35±0.5	0.35±0
5c	0.32±1.3	-0.31±0.6	0.36±0.2	0.99±0.6	-0.76±0	0.57±0.7	0.46±0.3	1.43±0.4	0.39±0.6	-0.14±0.5	0.24±0.4	0.34±0.1
5d	0.31±1.2	-0.37±0.5	nan	0.84±0.3	-0.77±0.2	0.35±0.5	0.32±0.2	1.31±0.4	0.26±0.5	-0.1±0.8	0.36±0.5	0.37±0.2
5e	0.47±1	-0.49±0.5	nan	0.75±0.7	-0.59±0.1	0.42±0.5	0.05±0.5	1.14±0.4	0.36±0.5	0.07±1.2	0.29±0.6	0.44±0.1

Table S5. Ocean CO_3^{2-} data (μmol kg^{-1}), mapped into SCP-M boxes and average for each MIS. Key to boxes: Atlantic (box 1: low latitude/tropical surface ocean; box 2: northern surface ocean; box 3: intermediate ocean; box 4: deep ocean; box 6: abyssal ocean; box 7: subpolar southern surface ocean). Pacific-Indian (box 8: low latitude/tropical surface ocean; box 9: deep ocean; box 10: abyssal ocean; box 11: subpolar southern surface ocean). Southern Ocean (box 5: intermediate-deep; box 12: surface ocean).

MIS	Box 1	Box 2	Box 3	Box 4	Box 5	Box 6	Box 7	Box 8	Box 9	Box 10	Box 11	Box 12
∼1	292.1±9	178.7±10	nan	116.6±5	nan	105.8±12	nan	nan	73.5±4	80.3±21	nan	nan
∼2	335±18	215.3±4	nan	144.7±3	nan	86.2±36	nan	nan	75.9±5	80.2±19	nan	nan
3	286.9±nan	nan	nan	135.6±6	nan	103.8±25	nan	nan	72.5±3	80.9±21	nan	nan
4	nan	nan	nan	nan	nan	80.5±16	nan	nan	66.3±4	70.9±14	nan	nan
5a	nan	nan	nan	nan	nan	102.2±11	nan	nan	71.9±8	nan	nan	nan
5b	nan	nan	nan	nan	nan	94.8±17	nan	nan	71.5±9	72.9±13	nan	nan
5c	nan	nan	nan	nan	nan	106.4±33	nan	nan	72.5±5	73.6±8	nan	nan
5d	nan	nan	nan	nan	nan	98.3±10	nan	nan	63.1±6	61.8±11	nan	nan
5e	nan	nan	nan	nan	nan	103.3±42	nan	nan	67.7±6	72.6±4	nan	nan

Data sourced from Yu et al. (2010), Yu et al. (2013), Yu et al. (2014b), Yu et al. (2014a), Broecker et al. (2015), Yu et al. (2016), Qin et al. (2017), Qin et al. (2018), Chalk et al. (2019).

Table S6. Ocean $\Delta^{14}C$ data (‰), mapped into SCP-M boxes and average for each MIS. Key to boxes: Atlantic (box 1: low latitude/tropical surface ocean; box 2: northern surface ocean; box 3: intermediate ocean; box 4: deep ocean; box 6: abyssal ocean; box 7: subpolar southern surface ocean). Pacific-Indian (box 8: low latitude/tropical surface ocean; box 9: deep ocean; box 10: abyssal ocean; box 11: subpolar southern surface ocean). Southern Ocean (box 5: intermediate-deep; box 12: surface ocean).

MIS	Box 1	Box 2	Box 3	Box 4	Box 5	Box 6	Box 7	Box 8	Box 9	Box 10	Box 11	Box 12
∼1	16.9±47	48.6±40	-66.9±109	27.7±99	nan	-31±124	-63.1±77	7.1±47	-80.4±76	-101.5±65	-6.6±58	nan
∼2	332.5±86	312.4±131	315.7±199	236.5±130	nan	73±202	243.4±151	320.6±146	153±176	67.2±174	315.8±116	nan
3	nan	nan	nan	nan	nan	236.8±93	499.1±36	413.1±112	404.8±123	-46.3±202	297.4±244	nan
4	nan	nan	nan	nan	nan	nan	nan	nan	nan	nan	nan	nan
5a	nan	nan	nan	nan	nan	nan	nan	nan	nan	nan	nan	nan
5b	nan	nan	nan	nan	nan	nan	nan	nan	nan	nan	nan	nan
5c	nan	nan	nan	nan	nan	nan	nan	nan	nan	nan	nan	nan
5d	nan	nan	nan	nan	nan	nan	nan	nan	nan	nan	nan	nan
5e	nan	nan	nan	nan	nan	nan	nan	nan	nan	nan	nan	nan

Data sourced from Skinner and Shackleton (2004), Marchitto et al. (2007), Barker et al. (2010), Bryan et al. (2010), Skinner et al. (2010), Burke and Robinson (2012), Davies-Walczak et al. (2014), Skinner et al. (2015), Chen et al. (2015), Hines et al. (2015), Sikes et al. (2016), Ronge et al. (2016), Skinner et al. (2017), Zhao et al. (2017).

3 Model-data experiment results

Table S7 shows the parameter values for global overturning circulation (GOC, Psi_1), Atlantic meridional overturning circulation (AMOC, Psi_2) and Southern Ocean biological export productivity (Z) from the model-data experiments described in the main text.

Table S7. Model-data experiment optimised values for ocean parameters in each MIS.

MIS	Psi_1 **(Sv)**	Psi_2 **(Sv)**	**Atlantic (Pacific-Indian) Southern Ocean** Z **(mol C m^{-2} yr^{-1}**
∼1	26	20	2.3 (0.8)
∼2	17	14	6.2 (2.2)
3	15	16	4 (1.4)
4	18	13	3.6 (1.3)
5a	18	19	3.2 (1.1)
5b	15	17	2.8 (1)
5c	17	20	2.8 (1)
5d	19	20	2.3 (0.8)
5e	28	20	3.6 (1.3)

Table S8 shows the optimised model-data experiment results for atmospheric CO_2, $\delta^{13}C$ and $\Delta^{14}C$, and the terrestrial biosphere.

Table S9 shows the optimised model-data experiment results for oceanic $\delta^{13}C$.

Table S10 shows the optimised model-data experiment results for oceanic CO_3^{2-}.

Table S11 shows the optimised model-data experiment results for oceanic $\Delta^{14}C$.

Table S8. Model-data experiment model results for atmospheric CO_2, atmospheric $\delta^{13}C$, atmospheric $\Delta^{14}C$, terrestrial biosphere net primary productivity (NPP) and carbon stock in each MIS.

MIS	**CO_2 (ppm)**	**$\delta^{13}C$ (‰)**	**$\Delta^{14}C$ (‰)**	Terrestrial biosphere NPP (PgC a^{-1})	Terrestrial biosphere carbon stock (PgC)
∼1	270.2	-6.4	38.2	72	2547.7
∼2	190.1	-6.42	518.6	50.7	1796.8
3	205.2	-6.54	454.8	52.1	1844.6
4	211.4	-6.7	194.4	52.9	1872.8
5a	241.2	-6.47	121.3	60	2123.2
5b	229.7	-6.47	126	57.8	2046
5c	242.1	-6.57	119.2	60.2	2130.6
5d	249.5	-6.68	106.9	59.5	2105.7
5e	275.8	-6.67	74.6	63.9	2262.2

Table S9. Model-data experiment model results for ocean $\delta^{13}C$ (‰) in each MIS. Key to boxes: Atlantic (box 1: low latitude/tropical surface ocean; box 2: northern surface ocean; box 3: intermediate ocean; box 4: deep ocean; box 6: abyssal ocean; box 7: subpolar southern surface ocean). Pacific-Indian (box 8: low latitude/tropical surface ocean; box 9: deep ocean; box 10: abyssal ocean; box 11: subpolar southern surface ocean). Southern Ocean (box 5: intermediate-deep; box 12: surface ocean).

MIS	**Box 1**	**Box 2**	**Box 3**	**Box 4**	**Box 5**	**Box 6**	**Box 7**	**Box 8**	**Box 9**	**Box 10**	**Box 11**	**Box 12**
∼1	2.92	2.74	1.94	1.12	1.08	0.57	1.99	3.22	0.58	0.32	2.63	2.19
∼2	3.27	3.08	2.09	0.53	0.55	-0.22	2.1	3.31	0.09	-0.63	3.27	1.91
3	3.03	2.81	1.9	0.63	0.59	-0.09	1.88	3.25	0.13	-0.66	3.04	1.85
4	3.07	2.97	1.91	0.63	0.64	0	1.98	3.22	0.2	-0.4	2.87	1.89
5a	2.92	2.7	1.88	0.86	0.8	0.19	1.87	3.21	0.3	-0.26	2.85	2.02
5b	2.96	2.75	1.85	0.76	0.69	0.07	1.84	3.26	0.22	-0.52	2.92	1.93
5c	2.8	2.56	1.78	0.83	0.75	0.16	1.77	3.12	0.24	-0.34	2.77	1.97
5d	2.76	2.54	1.75	0.86	0.78	0.23	1.76	3.07	0.28	-0.2	2.65	1.94
5e	2.69	2.53	1.75	0.88	0.86	0.33	1.82	2.9	0.35	0.14	2.46	2.02

Figure S1 shows the full range of experiments undertaken and the resulting model-data error mesh charts. These charts plot the difference between the model outputs and the proxy data, as a function of each of the three parameters varied in the model-data experiments (Psi_1, Psi_2 and Z).

Table S10. Model-data experiment model results for ocean CO_3^{2-} (μmol kg^{-1}) in each MIS. Key to boxes: Atlantic (box 1: low latitude/tropical surface ocean; box 2: northern surface ocean; box 3: intermediate ocean; box 4: deep ocean; box 6: abyssal ocean; box 7: subpolar southern surface ocean). Pacific-Indian (box 8: low latitude/tropical surface ocean; box 9: deep ocean; box 10: abyssal ocean; box 11: subpolar southern surface ocean). Southern Ocean (box 5: intermediate-deep; box 12: surface ocean).

MIS	Box 1	Box 2	Box 3	Box 4	Box 5	Box 6	Box 7	Box 8	Box 9	Box 10	Box 11	Box 12
∼1	268	202.8	180.9	113.3	110.6	85.5	152.8	258.3	98.8	88.8	175.7	142.1
∼2	341.2	256.4	242.5	124.4	129	85.4	203.5	320	117.9	88.7	232.5	181.5
3	325.5	241.4	228.5	127.1	127.8	85.5	189.9	311	116.2	88.7	220.4	173.7
4	316.7	236	219	118.2	121.4	85.4	182.7	297.3	111.1	88.8	209.6	167.2
5a	296.9	222	204.8	122.4	120.2	85.5	170.7	286.5	107.6	88.8	197.7	159.9
5b	309.5	231.6	214.1	125.1	123.3	85.5	177.9	297.8	111.3	88.7	207.1	164.7
5c	296.4	220.5	203.3	123.5	119.8	85.5	168.1	286.9	107.4	88.7	195.4	156
5d	285.9	213.5	194.6	120	116.2	85.5	160.6	276.4	104	88.7	186.1	149.7
5e	272.6	209.9	183.8	112.6	110.7	85.4	155.1	263.2	99.3	88.8	176.6	141.8

Table S11. Model-data experiment model results for ocean $\Delta^{14}C$ (‰) in each MIS. Key to boxes: Atlantic (box 1: low latitude/tropical surface ocean; box 2: northern surface ocean; box 3: intermediate ocean; box 4: deep ocean; box 6: abyssal ocean; box 7: subpolar southern surface ocean). Pacific-Indian (box 8: low latitude/tropical surface ocean; box 9: deep ocean; box 10: abyssal ocean; box 11: subpolar southern surface ocean). Southern Ocean (box 5: intermediate-deep; box 12: surface ocean).

MIS	Box 1	Box 2	Box 3	Box 4	Box 5	Box 6	Box 7	Box 8	Box 9	Box 10	Box 11	Box 12
∼1	-17.9	-22.2	-40.9	-73.9	-74.7	-106.5	-51.1	-32.8	-91.3	-139.1	-8.8	-33.8
∼2	376.2	363.6	314.2	223	222.3	157.3	288.1	344.8	196.5	75.3	402.2	301.1
3	368.2	363.3	309.4	230.5	226.4	160.3	286	348	199.3	61.4	407.7	303.7
4	99.2	91.1	61.6	0.4	0.5	-43.5	43.2	72.2	-17.1	-100.8	115.3	54.4
5a	35.2	30.7	6.7	-34.2	-36.5	-76.5	-6.2	20.4	-54.6	-132.1	59.6	12.5
5b	39.6	36.2	9.1	-37.3	-39.9	-82.6	-5.5	22	-57.6	-152.2	70.6	10.3
5c	31.7	27	4	-35.3	-37.9	-78.6	-8.3	18.5	-56.4	-138.4	60.1	12
5d	28	23.1	0.7	-38.1	-40.5	-79.3	-11.2	14.3	-58.6	-131.3	50.7	6.9
5e	11.7	6.7	-13	-47	-47.3	-79.9	-23.2	-3.6	-65.1	-110.4	18.2	-3.5

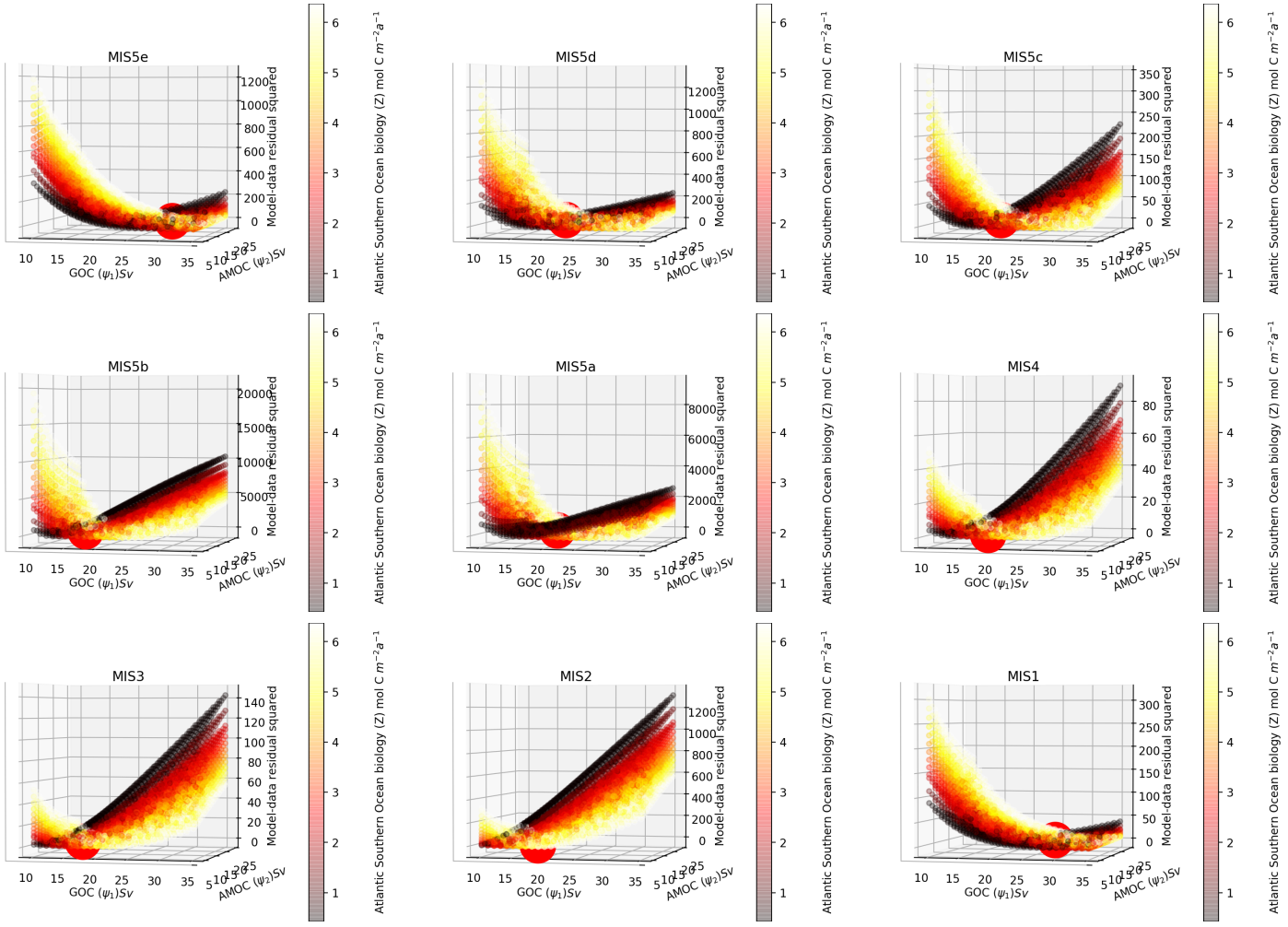

Figure S1. Model-data error surfaces for each of the model-data experiments within each MIS. The figures show the variation in the model-data residual, the "error" (the square of model results less data points) across the parameter input ranges for global overturning circulation (Ψ_1), Atlantic meridional overturning circulation (Ψ_2) and Atlantic Southern Ocean biological export productivity (Z). The latter (Z) is shown as the variations in colour of the data points, with the scale shown on the colour bar. The optimised values for the parameters are found at the bottom turning point of the curves, at the minimum of the model-data residual.

4 Model code and data

The model code, processed data files, model-data experiment results, and any (published) raw proxy data gathered in the course of this work, are located at https://doi.org/10.5281/zenodo.3559339. No original data was created, or unpublished data used, in this work. Figure S2 provides an overview of the files contained in the Zenodo repository, and their linkages. For more detail on the SCP-M equations, see O'Neill et al. (2019).

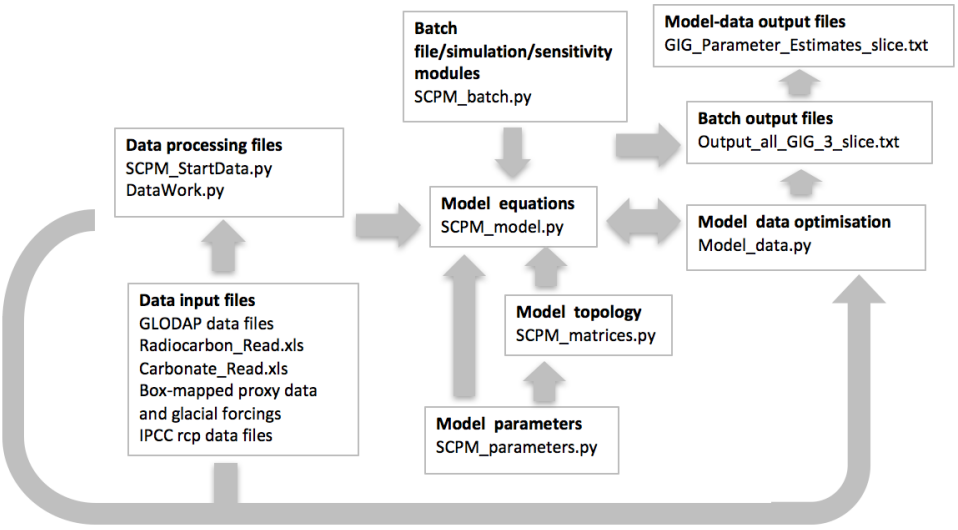

Figure S2. SCP-M files contained in the Zenodo repository at https://doi.org/10.5281/zenodo.3559339. The repository contains the model code and processed data files. Raw (published) data for carbonate ion proxy and $\Delta^{14}C$ gathered as part of the work is contained in spreadsheets in the data inputs folder. No new data was created, or unpublished data used, in this work.

References

Adkins, J., McIntyre, K., and Schrag, D.: The Salinity, Temperature, and 18O of the Glacial Deep Ocean, Science, 298, 1769–1773, 2002.

Barker, S., Knorr, G., Vautravers, M., Diz, P., and Skinner, L.: Extreme deepening of the Atlantic overturning circulation during deglaciation, Nature Geoscience, 3, 567–571, 2010.

Bereiter, B., Eggleston, S., Schmitt, J., Nehrbass-Ahles, C., Stocker, T., Fischer, H., Kipfstuhl, S., and Chappellaz, J.: Revision of the EPICA Dome C CO2 record from 800 to 600kyr before present, Geophys. Res. Lett, 2015.

Broecker, W., Yu, J., and Putnam, A.: Two contributors to the glacial CO2 decline, Earth and Planetary Science Letters, pp. 191–196, 2015.

Bryan, S., Marchitto, T., and Lehman, S.: The release of 14C-depleted carbon from the deep ocean during the last deglaciation: Evidence from the Arabian Sea, Earth and Planetary Science Letters, 298, 244–254, 2010.

Burke, A. and Robinson, L.: The Southern Ocean's Role in Carbon Exchange During the Last Deglaciation, Science, 335, 557–561, 2012.

Chalk, T., Foster, G., and Wilson, P.: Dynamic storage of glacial CO2 in the Atlantic Ocean revealed by boron [CO2-3] and pH records, Earth and Planetary Science Letters, 510, 1–11, 2019.

Chen, T., Robinson, L., Burke, A., Southon, J., Spooner, P., Morris, P., and Ng, H.: Synchronous centennial abrupt events in the ocean and atmosphere during the last deglaciation, Science, 349, 1537–1541, 2015.

Davies-Walczak, M., Mix, A., Stoner, J., Southon, J., Cheseby, M., and Xuan, C.: Late Glacial to Holocene radiocarbon constraints on North Pacific Intermediate Water ventilation and deglacial atmospheric CO2 sources, Earth and Planetary Science Letters, 397, 57–66, 2014.

Eggleston, S., Schmitt, J., Bereiter, B., Schneider, R., and Fischer, H.: Evolution of the stable carbon isotope composition of atmospheric CO2 over the last glacial cycle, Paleoceanography, 31, 434–452, 2016.

Hines, S., Southon, J., and Adkins, J.: A high-resolution record of Southern Ocean intermediate water radiocarbon over the past 30,000 years, Earth and Planetary Science Letters, 432, 46–48, 2015.

Key, R.: Ocean process tracers: Radiocarbon. In: Encyclopedia of Ocean Sciences, pp. 2338–2353, Academic Press, London, 2001.

Kohfeld, K. and Chase, Z.: Temporal evolution of mechanisms controlling ocean carbon uptake during the last glacial cycle, Earth and Planetary Science Letters, 472, 206–215, 2017.

Marchitto, T., Lehman, S., Ortiz, J., Flückiger, J., and van Geen, A.: Marine Radiocarbon Evidence for the Mechanism of Deglacial Atmospheric CO2 Rise, Science, 316, 1456–1459, 2007.

Muscheler, R., Beer, J., Wagner, G., Laj, C., Kissel, C., Raisbeck, G., Yioud, F., and Kubik, P.: Changes in the carbon cycle during the last deglaciation as indicated by the comparison of 10Be and 14C records, Earth and Planetary Science Letters, 219, 325–340, 2014.

Oliver, K., Hoogakker, B., Crowhurst, S., Henderson, G., Rickaby, R., Edwards, N., and Elderfield, H.: A synthesis of marine sediment core d13C data over the last 150 000 years, Climate of the Past, 6, 645–673, 2010.

O'Neill, C., A. Mc. Hogg, M.J. Ellwood, S. E., and Opdyke, B.: The [simple carbon project] model v1.0, Geosci. Model Dev., 12, 1541–1572, https://doi.org/10.5194/gmd–12–1541–2019, 2019.

Opdyke, B. and Walker, J.: Return of the coral reef hypothesis: Basin to shelf partitioning of CaCO3 and its effect on atmospheric CO2, Geology, 20, 733–736, 1992.

Qin, B., Li, T., Xiong, Z., Algeo, T. J., and Chang, F.: Deepwater carbonate ion concentrations in the western tropical Pacific since 250 ka: Evidence for oceanic carbon storage and global climate influence, Paleoceanography, 32, 351–370, 2017.

Qin, B., Li, T., Xiong, Z., Algeo, T., and Jia, Q.: Deep-Water Carbonate Ion Concentrations in the Western Tropical Pacific Since the Mid-Pleistocene: A Major Perturbation During the Mid-Brunhes, Journal of Geophysical Research: Oceans, 123, https://doi.org/10.1029/2018JC014 084, 2018.

Reimer, P., Baillie, M., Bard, E., Bayliss, A., Beck, J., Blackwell, P., Ramsey, C. B., Buck, C., Burr, G., Edwards, R., Friedrich, M., Grootes, P., Guilderson, T., Hajdas, I., Heaton, T., Hogg, A., Hughen, K., Kaiser, K., Kromer, B., McCormac, F., Manning, S., Reimer, R., Richards, D., Southon, J., Talamo, S., Turney, C., van der Plicht, J., and Weyhenmeyer, C.: IntCal09 and Marine09 radiocarbon age calibration curves, 0-50,000 years cal BP., Radiocarbon, 51, 1111–50, 2009.

Ridgewell, A., Watson, A., Maslin, M., and Kaplan, J.: Implications of coral reef buildup for the controls on atmospheric CO2 since the Last Glacial Maximum, Paleoceanography, 18, 1083, doi:10.1029/2003PA000 893, 2003.

Rohling, E., Grant, K., Bolshaw, M., Roberts, A., Siddall, M., Hemleben, C., and Kucera, M.: Antarctic temperature and global sea level closely coupled over the past five glacial cycles, Nature Geoscience, 2, 500–504, 2009.

Ronge, T., Tiedemann, R., Lamy, F., Kohler, P., Alloway, B., Pol-Holz, R. D., Pahnke, K., Southon, J., and Wacker, L.: Radiocarbon constraints on the extent and evolution of the South Pacific glacial carbon pool, Nature Communications, 7, 11 487, doi: 10.1038/ncomms11 487, 2016.

Sikes, E., Cook, M., and Guilderson, T.: Reduced deep ocean ventilation in the Southern Pacific Ocean during the last glaciation persisted into the deglaciation, Earth and Planetary Science Letters, 438, 130–138, 2016.

Skinner, L. and Shackleton, N. J.: Rapid transient changes in northeast Atlantic deep water ventilation age across Termination I, Paleoceanography, 19, PA2005, doi:10.1029/2003PA000 983, 2004.

Skinner, L., McCave, I., Carter, L., Fallon, S., Scrivner, A., and Primeau, F.: Reduced ventilation and enhanced magnitude of the deep Pacific carbon pool during the last glacial period, Earth and Planetary Science Letters, 411, 45–52, 2015.

Skinner, L., Primeau, F., Freeman, E., de la Fuente, M., Goodwin, P. A., Gottschalk, J., Huang, E., McCave, I. N., Noble, T. L., and Scrivner, A. E.: Radiocarbon constraints on the glacial ocean circulation and its impact on atmospheric CO2, Nature Communications, 8, 16 010, doi: 10.1038/ncomms16 010, 2017.

Skinner, L. C., Fallon, S., Waelbroeck, C., Michel, E., and Barker, S.: Ventilation of the Deep Southern Ocean and Deglacial CO2 Rise, Science, 328, 1147–1151, 2010.

Wolff, E., Barbante, C., Becagli, S., Bigler, M., Boutron, C., Castellano, E., de Angelis, M., Federer, U., Fischer, H., Fundel, F., Hansson, M., Hutterli, M., Jonsell, U., Karlin, T., Kaufmann, P., Lambert, F., Littot, G., Mulvaney, R., Roöthlisberger, R., Ruth, U., Severi, M., Siggaard-Andersen, M., Sime, L., Steffensen, J., Stocker, T., Traversi, R., Twarloh, B., Udisti, R., Wagenbach, D., and Wegner, A.: Changes in environment over the last 800,000 years from chemical analysis of the EPICA Dome C ice core, Quaternary Science Reviews, 29, 285–95, 2010.

Yu, J., Broecker, W., Elderfield, H., Jin, Z., McManus, J., and Zhang, F.: Loss of Carbon from the Deep Sea Since the Last Glacial Maximum, Science, 330, 1084–1087, 2010.

Yu, J., Anderson, R., Jin, Z., Rae, J., Opdyke, B., and Eggins, S.: Responses of the deep ocean carbonate system to carbon reorganization during the Last Glacial-interglacial cycle, Quaternary Science Reviews, 76, 39–52, 2013.

Yu, J., Anderson, R., Z.Jin, Menviel, L., Zhang, F., Ryerson, F., and Rohling, E.: Deep South Atlantic carbonate chemistry and increased interocean deep water exchange during last deglaciation, Quaternary Science Reviews, 90, 80–89, 2014a.

Yu, J., Anderson, R. F., and Rohling, E. J.: Deep ocean carbonate chemistry and glacial-interglacial atmospheric CO2 changes, Oceanography, 27, 16–25, 2014b.

Yu, J., Menviel, L., Jin, Z. D., Thornalley, D., Barker, S., Marino, G., Rohling, E. J., Cai, Y., Zhang, F., Wang, X., Dai, Y., Chen, P., and Broecker, W. S.: Sequestration of carbon in the deep Atlantic during the last glaciation, Nature Geoscience, 9, 319–325, 2016.

Zhao, N., Marchal, O., Keigwin, L., Amrhein, D., and Gebbie, G.: A Synthesis of Deglacial Deep-Sea Radiocarbon Records and Their (In)Consistency With Modern Ocean Ventilation, Paleoceanography and Paleoclimatology, 33, 128–151, 2017.